ECS Transactions, 9(1) 295-304 (2007)
10.1149/1.2766900©The Electrochemical Society

Electromigration Modeling for Interconnect Structures in Microelectronics

H. Ceric and S. Selberherr

Institute for Microelectronics, TU Vienna, Gußhausstraße 27–29, A-1040 Wien, Austria

Electromigration is one of the most important reliability issues in semiconductor technology. Its complex character demands comprehensive physical modeling as basis for analysis. Simulation of electromigration induced interconnect failure focuses on the life-cycle of intrinsic voids, which consists of two distinct phases: void nucleation and void evolution. We present models for both phases as well as models which describe the impact of metal microstructure and mechanical stresses. These stresses have their sources in the fabrication process itself and in the material transport caused by electromigration. Special emphasis is put on explaining the void morphology and its impact on interconnect resistance. Investigations for common two- and three-dimensional interconnect structures are presented. Implications of the theoretical analysis and the simulation results for modern interconnect design are discussed.

Introduction

Failure of metallic interconnects in integrated circuits caused by electromigration has long been a key reliability concern which is further accentuated by the continuing trend of miniaturization. The phenomenon of electromigration is a mechanism for transport of matter by high electric current densities which produce damage in the interconnect lines. Failure results either from voids growing over the entire line width or extrusions which cause short circuits to neighboring lines.

Copper with its lower resistivity, higher melting point, good mechanical strength, and better electromigration performance [1, 2] has replaced aluminum as advanced metalization solution. However copper based interconnects have introduced new problems, since copper electromigrates along fast diffusion paths at the interfaces to surrounding layers [3, 4].

The main challenge in electromigration modeling and simulation is the diversity of the relevant physical phenomena. Electromigration induced material transport is also accompanied by material transport driven by the gradients of material concentration, mechanical stress, and temperature. A comprehensive, physics based analysis of electromigration for modern copper interconnect lines serves as basis for deriving sophisticated design rules which will ensure higher steadfastness of interconnects against electromigration.

The material transport driven by electromigration is most commonly modeled by the dynamics of crystal vacancies. A high concentration of vacancies or high tensile stress indicates sites where the nucleation of intrinsic voids is very probable. The main

task of electromigration modeling and simulation is a prediction of the hot spots in the interconnect geometry where stress and vacancy concentration reach their peak values as well as the time needed for these values to be reached assuming usual operating conditions.

Electromigration Failure Mechanism

The development of intrinsic voids, which leads to interconnect failure, goes through two distinctive phases. These phases exhibit the different influence on the operating abilities of interconnects and are based on different physical phenomena.

The first phase is the void nucleating phase in which electromigration-generated voids do not exist and a significant resistance change is not observable. The second phase starts when a void is nucleated and becomes visible in SEM pictures [5]. This is the

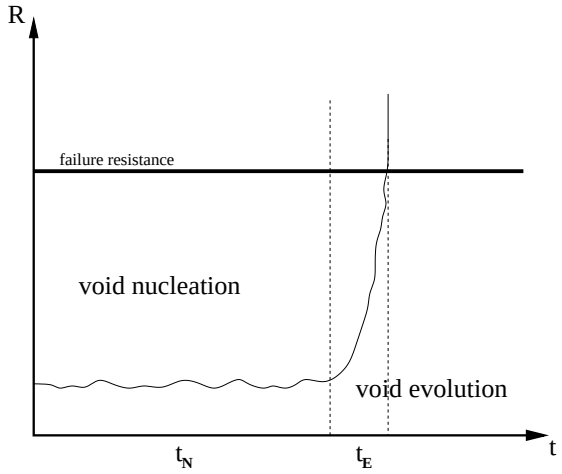

Figure 1: Resistance behavior and failure development phases.

so-called rapid phase of void development. The void expands from its initial position (nucleation site) to a size which can significantly change the resistance or completely sever the connection. If we denote the void nucleation time with t_N and the void evolution time with t_E, the time to failure t_F is,

$$t_F = t_N + t_E. \tag{1}$$

The expected resistance development during these time periods is sketched in Fig. 1. The development of a general electromigration model demands a careful analysis of physical phenomena in both phases of void development.

Void Nucleation

The electromigration model applied in this work is based on propositions made in [6]. The model connects the evolution of the mechanical stress with the diffusion of vacancies under full account of the influence of the geometry of the metalization.

The dynamics of the vacancies is described by the following two equations [6, 7]

$$\mathbf{J}_v = -D_v\Big(\frac{Z^*e}{k_B\,T}C_v\nabla\varphi + \nabla C_v + \frac{f\Omega}{3\,k_B\,T}C_v\nabla\,\mathrm{tr}(\sigma)\Big), \tag{2}$$

$$\frac{\partial C_v}{\partial t} = -\nabla \mathbf{J}_v + G(C_v), \tag{3}$$

where C_v is the vacancy concentration, f is the vacancy relaxation ratio, Ω is the atomic volume, D_v is the vacancy diffusivity, k_B is Boltzmann's constant, T is the local temperature, Z^*e is the effective valence, and $G(C_v)$ is the source function which models vacancy generation and annihilation processes. A closer look at equation (2) reveals that three major driving forces induce the dynamics of vacancies: the electromigration which is proportional to $\nabla\varphi$, the concentration gradient, and the mechanical stress gradient $\nabla \operatorname{tr}(\sigma)$.

If there is no residual mechanical stress from the technological process flow and an initially uniform distribution of vacancies (as is normally the case), it is obvious that the rise of mechanical stress and concentration gradients is a response to the electromigration stressing of the interconnect material. The overall behavior of temperature gradients depends on the material choice, the geometry of the interconnect layout, and the operating conditions. Both scenarios, in which temperature gradients enhance or retard vacancy transport induced by electromigration, are possible.

Considering the effective vacancy diffusivity we can distinguish between three basic diffusion paths and their diffusivities: bulk, grain boundaries, and copper interfaces to other layers. Interface self-diffusion is the dominant diffusion mechanism for the case of standard barrier layers such as TiN, as shown by many experimental observations [8, 9].

In his pioneering work on electromigration Korhonen *et al.* [10] use a direct relationship between lattice density and hydrostatic stress. This approach is based on simplifications which are justifiable only for a straight aluminum line. Other researchers, such as Povirk [11] and Rzepka *et al.* [12], searched for a more general description and employed the idea that diffusion fluxes give rise to volumetric strain which serves to establish stress fields, thereby driving stress-migration fluxes.

Using a similar concept, Sarychev and Zhitnikov [6] introduced a contribution of local vacancy dynamics to stress build-up in a three-dimensional model of stress evolution during electromigration. The standard elastic model was extended by introducing inelastic loads due to vacancy migration and recombination. The total strain tensor is given by

$$\varepsilon_{ik} = \varepsilon_{ik}^{v} + \varepsilon_{ik}^{\sigma}, \tag{4}$$

where ε_{ik}^{v} and $\varepsilon_{ik}^{\sigma}$ denote the inelastic and elastic strain component, respectively. The kinetic relation for inelastic strain component is given by [13],

$$\frac{\partial \varepsilon_{ij}^{v}}{\partial t} = \Omega\Big[(1-f)\nabla \mathbf{J}_v + f\frac{C_v - C_v^{eq}}{\tau}\Big]\delta_{ij}. \tag{5}$$

During the material redistribution induced by any driving force, the lattice actually tries to keep the vacancy concentration at its equilibrium value.

An even more complete model than this presented above also includes diffusion in the grain boundaries together with an interaction model which describes the vacancy exchange between the grain boundaries and the bulk. A model of this type was first studied by Fisher [14] and represents a promising improvement for electromigration modeling.

The lack of well-established models for nucleation of initial voids remains a limitation in modeling the failure of interconnect lines. Typically used nucleation conditions are critical stress or/and critical vacancy concentration [15], but in both cases it is actually very difficult to motivate values of these thresholds.

Consideration based on classical thermodynamics and kinetics [16] have shown that for aluminum, the nucleation rates for bulk, grain boundary, and sidewalls are very low. Such an analysis has, to the authors knowledge, not been carried out for copper technology.

Void Evolution

Modeling the micromechanics of void evolution is a long-standing scientific problem. It began with sharp interface models requiring an explicit finite element tracking of void surfaces during the course of evolution [17]. Later, prompted by the complexity of void surfaces, diffuse interface (DI) models were introduced [18, 19, 20].

Diffuse interface models circumvent computationally costly explicit surface tracking by application of a smooth order parameter field for the representation of void structures. An alternative diffuse interface model based on the double obstacle potential was proposed in [21], where the computation is simplified by reduction of order parameter profile evaluation to only the void-metal interfacial area.

The main disadvantages of these diffuse interface models are their requirement of underlying structured meshes for the order parameter evaluation and their restricted capability to reach higher resolution of an order parameter profile in the void-metal interfacial area.

In the case of void evolution there are two main forces which influence the shape of the evolving void interface: the chemical potential gradient and the electron wind. The first force causes self-diffusion of metal atoms on the void interface and tends to minimize energy, which results in circular void shapes. The electron wind force produces asymmetry in the void shape depending on the electrical field gradients.

Including both contributions, electromigration and chemical potential-driven surface diffusion, gives the total surface vacancy flux, $\mathbf{J_s} = J_s\mathbf{t}$, where $\mathbf{t}$ is the unit vector tangent to the void surface [17, 22]

$$J_s = -D_s\Big(eZ^*E_s + \Omega\nabla_s\Big(\frac{\sigma : \varepsilon}{2} - \gamma_s\kappa\Big)\Big). \tag{6}$$

$E_s \equiv \mathbf{E_s}\cdot\mathbf{t}$ is the local component of the electric field tangential to the void surface, ∇_s is the surface gradient operator, $0.5\,(\sigma : \varepsilon)$ is the strain energy density of the material adjacent to the void surface, and κ is the curvature of the void surface. D_s is given by an Arrhenius' law:

$$D_s = \frac{D_0\,\delta_s}{k_B\,T}\exp\Big(-\frac{Q_s}{k_B\,T}\Big). \tag{7}$$

Here, δ_s is the thickness of the diffusion layer, Q_s is the activation energy for the surface diffusion, and D_0 is the pre-exponential coefficient for mass diffusion. Equation (6) is the Nernst-Einstein equation, where the sum in the parentheses on the right side expresses the driving force. Mass conservation gives the void propagation velocity normal to the void surface, v_n, through the continuity equation,

$$v_n = -\nabla_s\mathbf{J_s}. \tag{8}$$

The full simulation scheme including void nucleation and void evolution is presented in Fig. 2. The simulation loops in the both phases (Fig. 2) are needed for a prediction of the time to failure of the interconect (1). The simulation in the second phase also determines resistance fluctuations.

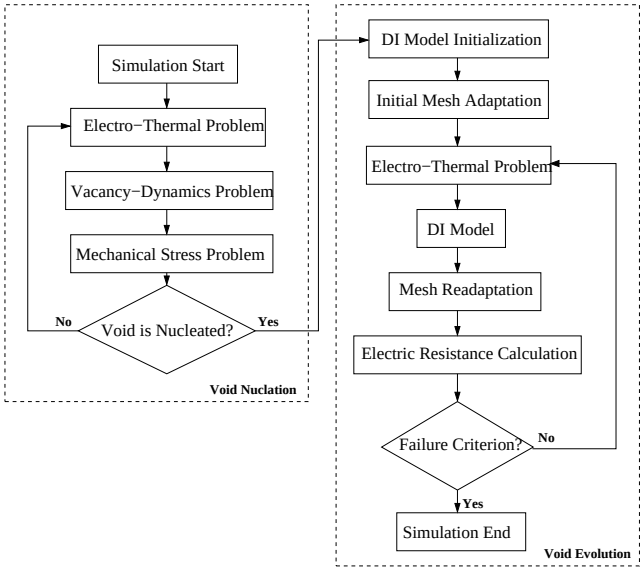

Figure 2: Two-phase electromigration simulation scheme.

Surface Tracking by Diffuse Interface Models

Direct numerical implementation of equations (6)-(8) demands explicit tracking of the moving void-metal interface. The interface is described by specifying a large number of points on it. Over the time the void-metal interface evolves and changes morphology and even more points may be required to accurately describe it. Such techniques are very complicated to implement and also tend to have rather poor numerical stability.
In the diffuse interface models void and metal area are presented through the order parameter ϕ which takes values $+1$ in the metal area, -1 in the void area and $-1 < \phi < +1$ in the void-metal interface area. Demanding explicit tracking of the void-metal interface is not needed and models do not require boundary conditions to be enforced at the moving boundary. Diffuse interface models are, as we will see in the next sections, quite simple to implement numerically.
The model equations for the void evolving in an unpassivated interconnect line are the balance equation for the order parameter ϕ [18, 21],

$$\frac{\partial \phi}{\partial t} = \frac{2D_s}{\epsilon \pi} \nabla \cdot (\nabla \mu - |e| Z^* \nabla V) \tag{9}$$

$$\mu = \frac{4\Omega \gamma_s}{\epsilon \pi} (f'(\phi) - \epsilon^2 \Delta \phi) \tag{10}$$

and for the electrical field

$$\nabla \cdot (\sigma(\phi) \nabla V) = 0 \tag{11}$$

where μ is the chemical potential, $f(\phi)$ is the double obstacle potential as defined in [23], and ϵ is a parameter controlling the void-metal interface width. The electrical conductivity was taken to vary linearly from the metal ($\sigma = \sigma_{metal}$) to the void area ($\sigma = 0$) by setting $\sigma = \sigma_{metal}(1 + \phi)/2$.

Simulation Results

In order to illustrate capabilities and consequences of the introduced models we consider two examples. The vacancy dynamics leading to void nucleation is studied for the case of a dual-damascene architecture consisting of copper, capping, and diffusion barrier layers, and void evolution for the case of a void nucleated in the bulk of the interconnect (Fig. 6). The structure was generated applying a typical damascene process flow using

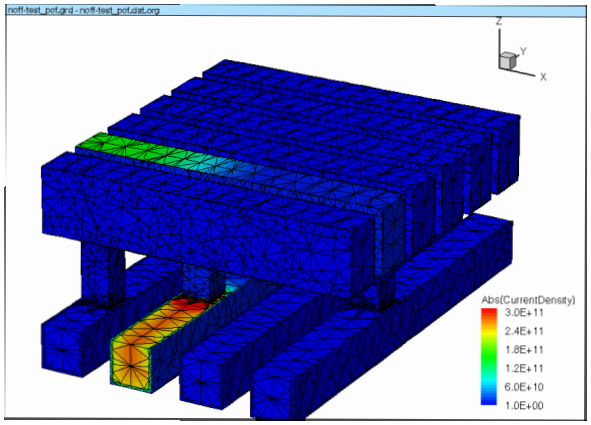

Figure 3: Current density distribution and applied finite element mesh.

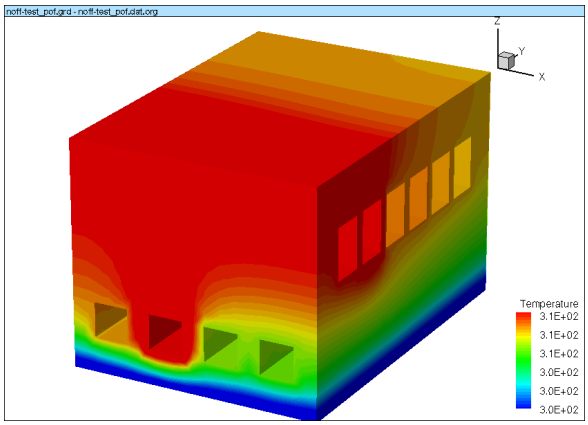

Figure 4: Temperature distribution.

DEP3D [24] for the deposition of the TiN barrier layer, copper, and dielectric (silicon-dioxide). For the emulation of the other deposition, etching, and polishing process steps, DEVISE [25] was used.

During the operation of the interconnect a redistribution of vacancies under the influence of the various promoting factors takes place. The increase of the vacancy concentration, i.e. depletion of material at specific places in the interconnect metal, leads to build-up of tensile stress. The simulated current density distribution together with the finite element mesh used is presented in Fig. 3 and the temperature distribution in Fig. 4.

Starting from uniformly distributed vacancies, during the operation of the interconnect local peaks of the vacancy concentration can be observed (Fig. 5). If a balance between electromigration, vacancy concentration, temperature, and mechanical stress gradients, which characterizes the operating condition of the interconnect, is reached, the vacancy concentration will remain at some value independent of time: the interconnect structure is virtually immortal. The interconnect layout and operating conditions chosen in the presented example produce a situation where the vacancy concentration remains stable at 6.5×10^{15} cm^{-3}. This concentration is well below the lattice sites concentration of 10^{23} cm^{-3}, but it still represents a supersaturation of approximately 3000 times the equilibrium value for 300° C.

As a setting for a void evolution example we consider a two-dimensional, stress free, electrically conducting interconnect via. A constant voltage is applied between points A and B (Fig. 6). At B a refractory layer is assumed. Because of geometrical reasons there is current crowding in the corners C and D. High electrical field gradients in the area around the corners increase the overall error of the finite element scheme, which is overcome by applying an additional refinement of the finite element mesh according to the

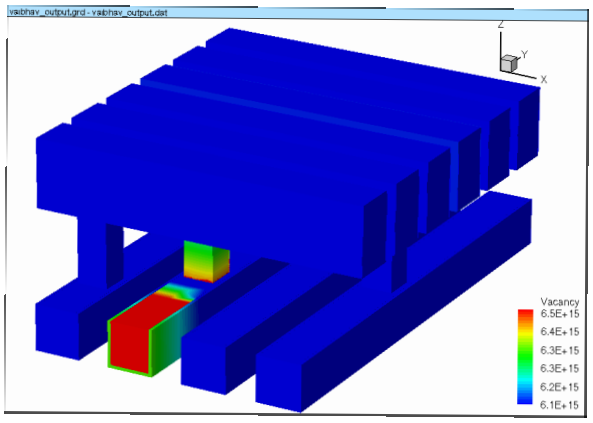

Figure 5: Electromigration induced vacancy distribution.

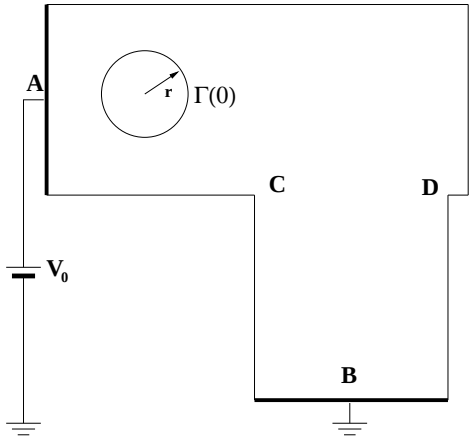

Figure 6: Interconnect via with initial void.

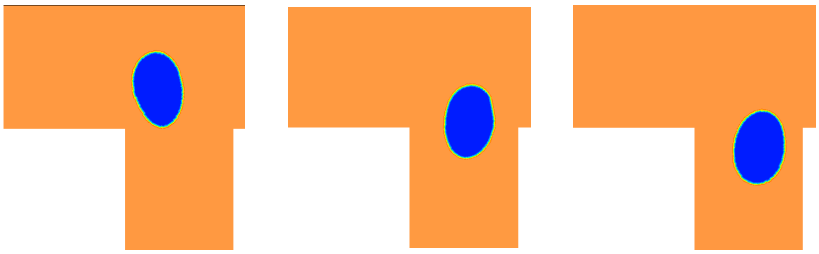

Figure 7: Void evolving through interconnect in the electric current direction

local value of the electric field. A fine triangulated belt area which is attached to the void-metal interface [22] at the initial simulation steps follows the interfacial area throughout the simulations, whereby the interconnect area outside the interface is coarsened to the level of the inital mesh.

In our simulations a void evolving through the straight part of the interconnect geometry exhibits similar shape changes as observed in earlier models [17]. There is also no significant fluctuation of the resistance during this period of void evolution (Fig. 8). The situation changes, when the void evolves in the proximity of the interconnect corner. Due to current crowding in this area the influence of the electromigration force on the material transport on the void surface is more pronounced than the influence of the chemical potential gradient. This leads to higher asymmetry in the void shape then observed in the straight part of the interconnect. A void evolving in the proximity of the interconnect corner causes significant fluctuations in the interconnect resistance due to asymmetry and position. The resistance change shows a charasteristic profile with two peaks and a valley (Fig. 8).

The extremes are more pronounced for larger initial voids. The capability of the applied adaptation scheme is also presented in the simulation of void collision with the interconnect refractory layer (Fig. 9).

Our simulations shows that for all considered initial void radii, voids follow the electric current direction (Fig. 9) and do not transform in slit or wedge like formations which have been found to be the main cause for complete interconnect failure [26].

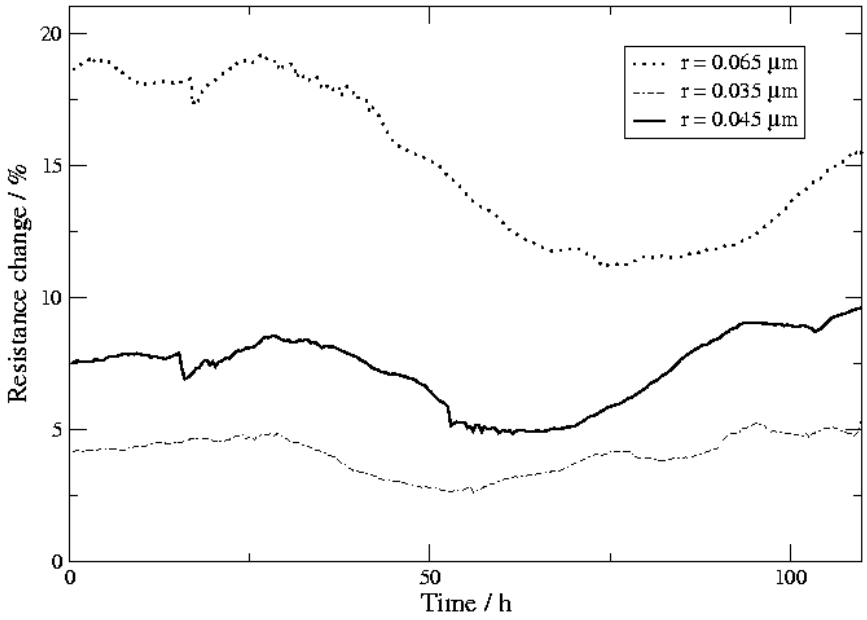

Figure 8: Time dependent resistance change during void evolution for the different initial void radius r.

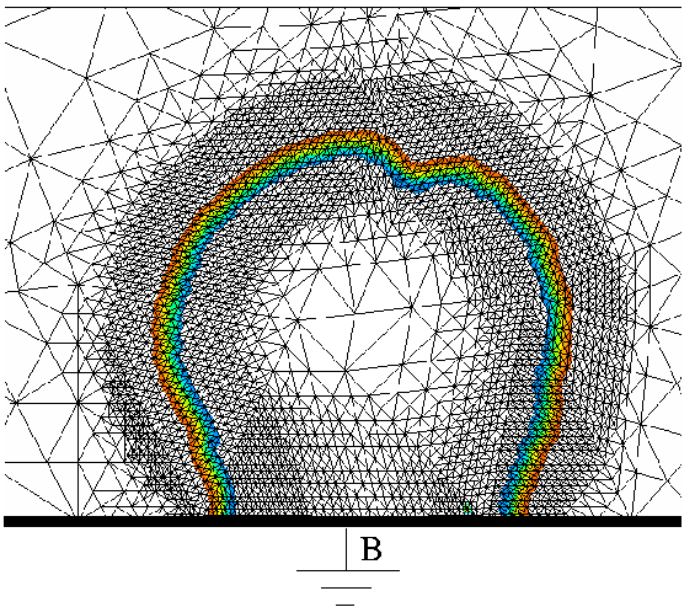

Figure 9: Mesh adaptation in the case of void collision with the refractory layer.

The applied diffuse interface model extends readily to incorporate additional physical phenomena such as anisotropy, temperature variations, and bulk and grain boundary diffusion.

Conclusion and Outlook

The electromigration reliability analysis of modern inteconnects demands simulation tools which are based on comprehensive physical models. In order to predict an interconnect failure, modeling and analysis of complete life cycles of electromigration induced intrinsic voids are needed.

A careful analysis of the connection between the local vacancy dynamics and strain build-up must be carried out. The obtained relations have been coupled to an electromigration model using the concepts of stress driven diffusion and anisotropy of the diffusivity tensor. For correct physical handling of the grain boundary network as the network of high diffusivity paths and at the same time as sites of vacany recombination, a method of splitting a copper segment into grain segments is introduced. The grain boundary segments are treated as simulation sub-domains connected to each other by diffusive, mechanical, and electrical interface conditions. A dual-damascene architecture example layout is used to illustrate and verify the introduced modeling approach. The obtained simulation results qualitatively resemble the behavior observed in experimental investigations.

A governing equation for the void evolution is solved using the finite element scheme. A dynamically adapted mesh is maintained by a refinement-coarsening algorithm controlled by position, curvature, and width of the simulated void-metal interface, which distributes the mesh density in such a way, that it allows efficient simulation of evolving voids through large portions of a complex interconnect geometry. Due to high electrical current gradients in the proximity of the interconnect corners and overall asymmetry of the electrical field, voids exhibit a specific faceting which was not observed in the case of straight interconnect geometries.

The presented method is well suited for long time prediction of resistance change due to electromigration during the interconnect life time. The applied diffuse interface model can be extended readily to incorporate additional physical phenomena such as anisotropy, temperature variations, and bulk and grain boundary diffusion.

Acknowledgment

This work has been supported by the Austrian Science Fund (FWF) with the project P18825-N14.

References

[1] R. H. Havemann, and J. A. Hutchby, *Proceedings of the IEEE* **89**, 586 – 601 (2001).

[2] S. Yokogawa, N. Okada, Y. Kakuhara, and H. Takizawa, *Microelectron. Reliab* **41**, 1409–1416 (2001).

[3] C. Hu, and J. Harper, *Mater. Chem. Phys* **52**, 5–16 (1998).

[4] L. Arnaud, T. Berger, and G. Reimbold, *J. Appl. Phys.* **93**, 192–204 (2003).

[5] M. A. Meyer, I. Zienert, and E. Zschech, *Materials for Information Technology* **1**, 95–100 (2005).

[6] M. E. Sarychev, and Y. V. Zhitnikov, *J. Appl. Phys.* **86**, 3068 – 3075 (1999).

[7] H. Ye, C. Basaran, and D. Hopkins, *IEEE Trans. on Comp. and Pack.* **26**, 673 – 681 (2003).

[8] N. Meier, T. Marieb, P. Flinn, R. Gleixner, and J. Bravman, *Proc. American Institute of Physics Conference* pp. 180–185 (1999).

[9] M. A. Meyer, M. Herrmann, E. Langer, and E. Zschech, *Microelectronic Engineering* **64**, 375–382 (2002).

[10] M. A. Korhonen, P. Borgesen, K. N. Tu, and C. Y. Li, *J. Appl. Phys.* **73**, 3790–3799 (1993).

[11] G. L. Povirk, *Proc. Mater. Res. Soc. Symp.* **473**, 327–342 (1997).

[12] S. Rzepka, M. A. Korhonen, E. R. Weber, and C. Y. Li, *Proc. Mater. Res. Soc. Symp.* **473**, 329–335 (1997).

[13] H. Ceric, R. Heinzl, C. Hollauer, T. Grasser, and S. Selberherr, *Stress-Induced Phenomena in Metallization, AIP* pp. 262–268 (2006).

[14] J. C. Fisher, *J. Appl. Phys.* **22**, 74–77 (1951).

[15] V. Sukharev, *Stress-Induced Phenomena in Metallization: 8th International Workshop, AIP Conference Proceedings, this volume* (2005).

[16] R. J. Gleixner, B. M. Clemens, and W. D. Nix, *Journal of Materials Research* **12**, 2081–2090 (1997).

[17] D. R. Fridline, and A. F. Bower, *J. Appl. Phys.* **85**, 3168–3174 (1999).

[18] M. Mahadevan, and R. Bradley, *Phys. Rev. B* **59**, 11037–11046 (1999).

[19] M. Mahadevan, and R. Bradley, *Physica D* **126**, 201–213 (1999).

[20] M. Mahadevan, R. Bradley, and J. M. Debierre, *Europhys. Lett.* **45**, 680–685 (1999).

[21] D. N. Bhate, A. Kummar, and A. F. Bower, *J. Appl. Phys.* **87**, 1712–1721 (2000).

[22] H. Ceric, and S. Selberherr, *IEICE Trans. Electronics* pp. 421–426 (2002).

[23] J. Blowey, and C. Elliott, *European Journal of Applied Mathematics* **3**, 147–179 (1992).

[24] E. Baer, J. Lorenz, and H. Ryssel, *Microelectr. Eng.* **64**, 321 – 328 (2002).

[25] *Synopsys Switzerland Ltd., Switzerland* (2004).

[26] E. Arzt, O. Kraft, W. D. Nix, and J. E. Sanchez, *J. Appl. Phys.* **76**, 1563–1571 (1994).